Smart Structures and Systems, *Vol. 19, No. 5 (2017) 567-576*
DOI: https://doi.org/10.12989/sss.2017.19.5.567

A new broadband energy harvester using propped cantilever beam with variable overhang

R. Usharani[1a], G. Uma[*2], M. Umapathy[2b] and S.B. Choi[3c]

[1]*Department of Instrumentation and Control Engineering, Seshasayee Institute of Technology, Tiruchirappalli,Tamilnadu ,India. 620010*
[2]*Department of Instrumentation and Control Engineering, National Institute of Technology, Tiruchirappalli, Tamilnadu ,India. 620015*
[3]*Department of Mechanical Engineering, Inha University, Incheon, Korea*

(Received August 29, 2016, Revised April 11, 2017, Accepted April 18, 2017)

Abstract. Design of piezoelectric energy harvester for a wide operating frequency range is a challenging problem and is currently being investigated by many researchers. Widening the operating frequency is required, as the energy is harvested from ambient source of vibration which consists of spectrum of frequency. This paper presents a new technique to increase the operating frequency range which is achieved by designing a harvester featured by a propped cantilever beam with variable over hang length. The proposed piezoelectric energy harvester is modeled analytically using Euler Bernoulli beam theory and the effectiveness of the harvester is demonstrated through experimentation. The results from analytical model and from experimentation reveal that the proposed energy harvester generates an open circuit output voltage ranging from 36.43 V to 11.94 V for the frequency range of 27.24 Hz to 48.47 Hz. The proposed harvester produces continuously varying output voltage and power in the broadened operating frequency range.

Keywords: broadband; energy harvester; piezoelectric; propped beam; resonance; vibration

1. Introduction

Energy harvesting from ambient vibrations in the environment using piezoelectric materials has been the area of interest for many researchers in the last decade. Low power electronic devices, wireless sensors, machine condition monitoring sensors, implantable devices etc will harvest energy from their operating environment for their operation. Review of energy harvesting from mechanical vibrations using piezoelectric materials and the harvesting devices developed are reported by Kim *et al.* (2011), Anton and Sodano (2007) and Beeby *et al.* (2006).

The ambient vibration in the environment in general consists of a spectrum of frequency. Hence the application of energy harvesters designed to operate at a particular frequency is highly limited as it produces maximum output only at that frequency. To overcome this limitation, energy harvesters are designed to operate in broadband. The broadband energy harvesting techniques are reviewed and presented by Zhu *et al.* (2010) and Tang *et al.* (2010).

The use of cantilever array to increase the bandwidth is reported by Shahruz (2008), the resonant frequencies are adjusted by tuning the geometry or by applying proof mass. A novel design for broadband piezoelectric energy harvester using multiple piezoelectric bimorphs with different aspect ratios is proposed by Xue *et al.* (2008) and concluded that the operating frequency band can be tailored by choosing appropriate connection pattern among the piezoelectric bimorphs. A double mass piezoelectric cantilever beam based energy harvester is modeled and experimental investigations are carried out by Ou *et al.* (2012) and shown that the proposed harvester is simple and provide reliable solution to widen the bandwidth as compared with the other broadband energy harvesters that involve moving parts and control electronics. A broad band piezoelectric energy harvester using L shaped beam mass structure having the first two natural frequencies closer to each other as compared to the conventional cantilever beam is designed by Erturk *et al.* (2009). Two elastically and electrically connected piezoelectric beams whose resonance frequencies are very close to each other and also adjustable is proposed by Yang and Yang (2009) for obtaining wider frequency range. A magnet induced dual cantilever piezoelectric energy harvester is designed by Su *et al.* (2014) and demonstrated that it can generate higher power output at wide bandwidth as compared to the simple cantilever piezoelectric energy harvester. A piezoelectric vibration energy harvester with a multimode dynamic magnifier is proposed by Zhou *et al.* (2012) and demonstrated that more energy can be harvested in the wider frequency range. A

*Corresponding author, Associate Professor
E-mail: guma@nitt.edu
[a] Lecturer
E-mail: ushar.69@gmail.com
[b] Professor
E-mail: umapathy@nitt.edu
[c] Professor
E-mail: seungbok@inha.ac.kr

ISSN: 1738-1584 (Print), 1738-1991 (Online)

new two degree of freedom piezoelectric energy harvester to provide larger bandwidth is proposed by Wu *et al.* (2013) as compared to the conventional single degree of freedom. The design consists of main cantilever beam and inner secondary cantilever beam, the first two resonant frequencies of the harvester can be tuned to achieve the useful wide bandwidth by varying the proof mass placed in the inner cantilever beam. A broadband piezoelectric energy harvester which consists of a clamped-clamped main beam with small cantilevers attached to both sides of the main beam is designed by Qi *et al.* (2010) in which the small cantilevers induce multi resonant response in the main beam. A novel energy harvester using low Young's modulus flexible frame and inter digital structure cantilever is proposed by Li *et al.* (2015) and demonstrated that an increase in bandwidth of the energy harvester as compared to the harvester designed with cantilever. Kim *et al.* (2011) designed piezoelectric energy harvester based on 2 degrees of freedom vibration (translation and rotation of single mass) and shown that the bandwidth is greater than the conventional single degree of freedom harvester. Niri and Salamone (2012) reported a dual cantilever piezoelectric energy harvester with variable tip stiffness and axial load and proposed a novel sliding mechanism to widen the resonant frequency of the device. Zhu *et al.* (2013) used a simply supported piezoelectric beam and shown that dynamic compressive loading provides relatively large amplitude response over a wide frequency range. Peters *et al.* (2009) designed a piezoelectric energy harvester with a tunable mechanism to adjust the resonant frequency by stiffening the structure using piezoelectric actuators. A self adaptive electromagnetic energy harvesting system is proposed by Hoffmann *et al.* (2016) and demonstrated that the system can self-adjust its Eigen frequency. A two dimensional tunable vibration based energy harvesting device is proposed by Dong *et al.* (2016) which uses two dimensional magnetic stiffness tuning method.

Consequently, the technical originality of this work is to introduce a new broadband piezoelectric energy harvester using the propped cantilever beam with variable overhang length. The proposed method is the first approach of its kind to broaden the operating frequency range. The proposed harvester structure is simple in design and easy to fabricate, since it does not involve any additional mass, beams, bimorph piezoelectric etc. In most of the works, Ou *et al.* (2012), Niri and Salamone (2012) reported in the area of the broadband piezoelectric energy harvester, the output is intermittently high at the few operating frequency in the broadened frequency range. However, in this proposed work, the harvester provides continuously and gradually varying output voltage in the operating frequency range. Simple mechanical means can be devised to move the support with the ambient vibration frequency variation without additional power requirement. Those described in the above are main technical contributions of this work in the energy harvesting research area utilizing piezoelectric materials. This paper is organized as follows: section 2 describes the structure of the proposed energy harvester and its principle. The model of the energy harvester is presented in section 3. Results from the analytical model and experimentation are discussed in sections 4 and 5. Conclusions are given in section 6.

2. Description of the proposed energy harvester

The schematic of the broadband energy harvester structure designed using propped cantilever beam with overhang length and the detailed description of section II and V are shown in Figs. 1(a) and 1(b). The overhang length can be varied by changing the position of the support P placed at a distance of L_3 from the fixed end. The resonant frequency of the energy harvester can be tuned by varying the position of the support P. Two piezoelectric patches of length l_p are bonded on the top surface of the beam, one at a distance of L_1 and another at L_4 from the fixed end. The use of two piezoelectric patches helps to improve the amplitude of the harvested voltage in the operating frequency range (broadband). The performance of the proposed energy harvester is demonstrated by exciting the harvester with an electromagnetic exciter placed at the free end of the beam (Santhosh kumar *et al.* 2012).

3. Modeling of the energy harvester

The model of the energy harvester in Fig. 1(a) is developed using Euler Bernoulli beam theory. The structure of the energy harvester is split into six sections namely sections I-VI as shown in Fig. 1(a). The governing equation of motion for the Euler Bernoulli beam with variable parameters under the tip dynamic force $f(x,t)$ is given by (Erturk and Inman 2008)

$$\frac{\partial^2 M(x,t)}{\partial x^2} + c(x)\frac{\partial w^{(r)}(x,t)}{\partial t} + m(x)\frac{\partial^2 w^{(r)}(x,t)}{\partial t^2} = f(x,t) \quad (1.1)$$

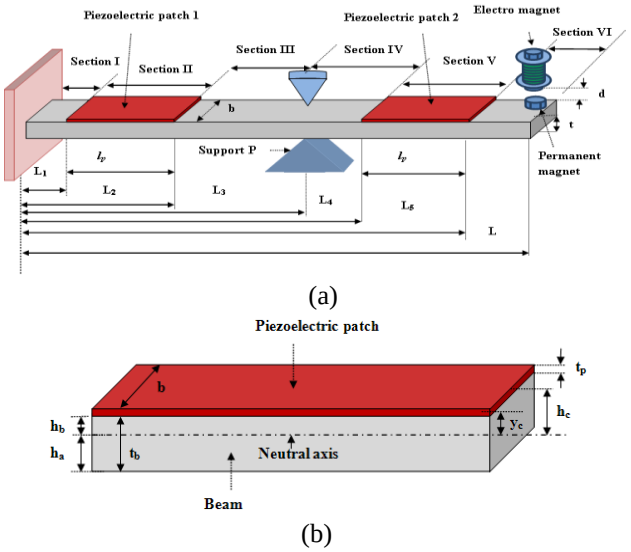

Fig. 1 (a) Schematic of the proposed energy harvester and (b) Detailed description of Sections II and V

$$\text{with} \quad M(x,t) = E(x)I(x)\frac{\partial^2 w^{(r)}(x,t)}{\partial x^2} + \vartheta v(t) \quad (1.2)$$

where $M(x,t)$, $c(x)$, $m(x)$, $E(x)$ and $I(x)$ are the internal bending moment, variable damping coefficient, mass per unit length, stiffness and moment of inertia respectively. $w^{(r)}(x,t)$ is the transverse vibratory displacement function for the r^{th} mode, $v(t)$ is the voltage across the piezoelectric patch and ϑ is the coupling term. The damping is assumed to be uniform for all the sections of the harvester. For obtaining the natural frequencies and the mode shapes of the harvester, free and undamped conditions associated with the transverse vibration of the harvester is used and is given by

$$\frac{\partial^2 M(x,t)}{\partial x^2} = -m(x)\frac{\partial^2 w^{(r)}(x,t)}{\partial t^2} \quad (2)$$

The free vibration solution of Eq. (2) is found by using the method of separation of variables as

$$w(x,t) = \sum_{r=1}^{\infty} W^{(r)}(x)T^{(r)}(t) \quad (3)$$

where $W^{(r)}(x)$ denotes the spatial mode shape function, $T^{(r)}(t)$ represents the generalized time dependent coordinate for the r^{th} mode.

3.1 Modal analysis of the energy harvester

The spatial mode shape function for the free undamped vibration of Eq. (2) is

$$\frac{d^2}{dx^2}\left(E(x)I(x)\frac{d^2W^{(r)}(x)}{dx^2}\right) = \omega_r{}^2 m(x)W^{(r)}(x) \quad (4)$$

where ω_r is the r^{th} mode natural frequency of the harvester. Mode shapes and mode frequencies of the harvester are obtained by solving the Eq. (4). The flexural rigidity $E(x)I(x)$ and mass $m(x)$ for the sections I-VI in Fig. 1 (a) of the proposed harvester are given by

$$E(x)I(x) = \begin{cases} (EI)_i & L_{i-1} \le x \le L_i,\ i = 1,3,4,6 \\ (EI)_j & L_{j-1} \le x \le L_j,\ j = 2,5 \end{cases} \quad (5.1)$$

$$m(x) = \begin{cases} m_i & i = 1,3,4,6 \\ m_j & j = 2,5 \end{cases} \quad (5.2)$$

As sections I, III, IV and VI have only beam element with uniform dimensions, the flexural rigidity $(EI)_i$ and the mass per unit length m_i are constant and are given by

$$(EI)_i = E_b I_b,\ \ m_i = \rho_b b t_b,\ \ I_b = \frac{bt_b^3}{12} \quad (6)$$

E_b, ρ_b and b are the Young's modulus, density and width of the beam respectively. t_b is the beam thickness at i=1,3,4,6 and I_b represents the moment of inertia for aforementioned sections. The flexural rigidity $(EI)_j$ and the mass per unit length m_j for sections II, V are given by

$$\begin{gathered} m_j = b\left[\rho_b t_b + \rho_p t_p\right], \\ (EI)_j = \frac{b}{3}\left[E_b\left(h_b^3 - h_a^3\right) + E_p\left(h_c^3 - h_b^3\right)\right],\ j = 2,5 \end{gathered} \quad (7.1)$$

where E_p, ρ_p, b and t_p are the Young's modulus, density, width and thickness of the piezoelectric patch. h_a is the position of the bottom layer of the beam from the neutral axis (always negative), h_b is the position of the top layer of the beam from the neutral axis (positive or negative), h_c is the position of the top layer of the piezoelectric patch from the neutral axis (always positive), η is the ratio of Young's moduli, y_c is the distance from the center of the piezoelectric patch to the neutral axis and are given by

$$\begin{gathered} h_a = -\left[\frac{t_p^2 + 2t_p t_b + \eta t_b^2}{2\left(t_p + \eta t_b\right)}\right],\ h_b = \frac{\eta t_b^2 - t_p^2}{2\left(t_p + \eta t_b\right)}, \\ h_c = \frac{t_p^2 + 2\eta t_p t_b + \eta t_b^2}{2\left(t_p + \eta t_b\right)} \end{gathered} \quad (7.2)$$

$$y_c = \frac{\eta t_b\left(t_p + t_b\right)}{2\left(t_p + \eta t_b\right)},\ \ \eta = \frac{E_b}{E_p} \quad (7.3)$$

Using the Eqs. (5)-(7), Eq. (4) is modified as

$$(EI)_n\frac{d^2W_n^{(r)}(x)}{dx^2} = \omega_r{}^2 m_n W_n^{(r)}(x),\quad L_{n-1} \le x \le L_n \quad (8)$$

where $n = 1,2,\ldots 6$ $\qquad L_0 = 0$, $L_6 = L$

The free vibration solution for Eq. (8) is given by

$$W_n^{(r)}(x) = A_n^{(r)}\sin\beta_n^{(r)}x + B_n^{(r)}\cos\beta_n^{(r)}x + C_n^{(r)}\sinh\beta_n^{(r)}x + D_n^{(r)}\cosh\beta_n^{(r)}x \quad (9.1)$$

$$\text{where} \quad \beta_n^{(r)4} = \frac{\omega_r^2 m_n}{(EI)_n},\ n = 1,2,\ldots 6 \quad (9.2)$$

$A_n^{(r)}, B_n^{(r)}, C_n^{(r)}, D_n^{(r)}$ are the constants of integration for the r^{th} mode and are obtained by solving the characteristic equation of the harvester, by applying the following boundary and continuity conditions (Salehi-Khojin *et al.* 2008).

The clamped-free beam boundary conditions are

$$\text{At} \quad x = 0,\quad W_1^{(r)}(0) = 0,\ \ \frac{dW_1^{(r)}(0)}{dx} = 0 \quad (10.1)$$

$$\text{At} \quad x = L,\ \ \frac{d^2W_6^{(r)}(L)}{dx^2} = 0,\ \ \frac{d^3W_6^{(r)}(L)}{dx^3} = 0 \quad (10.2)$$

The continuity conditions at $x=L_q$, where $q= 1, 2, 4, 5$ are

$$W_q^{(r)}\left(L_q\right)=W_{q+1}^{(r)}\left(L_q\right),\ \frac{dW_q^{(r)}\left(L_q\right)}{dx}=\frac{dW_{q+1}^{(r)}\left(L_q\right)}{dx} \quad (10.3)$$

$$\left(EI\right)_q\frac{d^2W_q^{(r)}\left(L_q\right)}{dx^2}=\left(EI\right)_{q+1}\frac{d^2W_{q+1}^{(r)}\left(L_q\right)}{dx^2} \quad (10.4)$$

$$\left(EI\right)_q\frac{d^3W_q^{(r)}\left(L_q\right)}{dx^3}=\left(EI\right)_{q+1}\frac{d^3W_{q+1}^{(r)}\left(L_q\right)}{dx^3} \quad (10.5)$$

The continuity conditions at the support $x=L_3$ are (Murphy 1997)

$$W_3^{(r)}\left(L_3\right)=W_4^{(r)}\left(L_3\right)=0 \quad (10.6)$$

$$\frac{dW_3^{(r)}\left(L_3\right)}{dx}=\frac{dW_4^{(r)}\left(L_3\right)}{dx} \quad (10.7)$$

$$\left(EI\right)_3\frac{d^2W_3^{(r)}\left(L_3\right)}{dx^2}=\left(EI\right)_4\frac{d^2W_4^{(r)}\left(L_3\right)}{dx^2} \quad (10.8)$$

Applying the boundary and continuity conditions Eqs. (10.1)-(10.8) into Eq. (9.1), the characteristics matrix equation of the harvester is formed. In Eq. (9.2), the $\beta_n^{(r)}$'s are functions of natural frequency of the harvester. The natural frequency is independent of sections and the natural frequency considered is for the entire harvester $\beta_n^{(r)}$'s of the individual section can be written in terms of a single parameter $\beta^{(r)}$

$$\beta_n^{(r)}=\beta^{(r)}\alpha_n,\ \ n=1,2,...6$$

$$\text{where } \alpha_n=\left(\frac{m_n\left(EI\right)_1}{m_1\left(EI\right)_n}\right)^{\frac{1}{4}},\ \alpha_1=1 \text{ and } \beta^{(r)}=\beta_1^{(r)}. \quad (11)$$

Therefore characteristics matrix becomes only function of a single parameter $\beta^{(r)}$. The characteristics equation is given by

$$K_{24\times24}P_{24\times1}=0 \quad (12.1)$$

where $K=K(\beta^{(r)})$ is the characteristic matrix and P is the vector of mode shape coefficients.

$$P=\left[A_1^{(r)}\ B_1^{(r)}\ C_1^{(r)}\ D_1^{(r)}\ A_2^{(r)}\ B_2^{(r)}\ C_2^{(r)}\ D_2^{(r)}\ .....\ A_6^{(r)}\ B_6^{(r)}\ C_6^{(r)}\ D_6^{(r)}\right]^T \quad (12.2)$$

The $\beta^{(r)}$ values and the natural frequencies for all modes are obtained by setting the determinant of the characteristics matrix to zero.

$$K(\beta^{(r)})=0 \quad (12.3)$$

where $K(\beta^{(r)})$ is a 24 × 24 matrix.

3.2 Forced vibration analysis of the harvester

The expression for the transversal displacement for the beam vibration analysis based on the expansion theorem is

$$w(x,t)=\sum_{r=1}^{\infty}W^{(r)}\left(x\right)T^{(r)}\left(t\right) \quad (13)$$

where $W^{(r)}\left(x\right)$ is the r^{th} mode shape of the harvester, $T^{(r)}\left(t\right)$ is the generalized time dependent coordinate of r^{th} mode to be determined by substituting Eq. (13) in Eq. (1.1). $W^{(r)}\left(x\right)$ is given by

$$\begin{aligned}
W_1^{(r)}(x)&=A_1^{(r)}\sin\beta_1^{(r)}x+B_1^{(r)}\cos\beta_1^{(r)}x+C_1^{(r)}\sinh\beta_1^{(r)}x+D_1^{(r)}\cosh\beta_1^{(r)}x,\ 0\le x\le L_1\\
W_2^{(r)}(x)&=A_2^{(r)}\sin\beta_2^{(r)}x+B_2^{(r)}\cos\beta_2^{(r)}x+C_2^{(r)}\sinh\beta_2^{(r)}x+D_2^{(r)}\cosh\beta_2^{(r)}x,\ L_1\le x\le L_2\\
W_3^{(r)}(x)&=A_3^{(r)}\sin\beta_3^{(r)}x+B_3^{(r)}\cos\beta_3^{(r)}x+C_3^{(r)}\sinh\beta_3^{(r)}x+D_3^{(r)}\cosh\beta_3^{(r)}x,\ L_2\le x\le L_3\\
W_4^{(r)}(x)&=A_4^{(r)}\sin\beta_4^{(r)}x+B_4^{(r)}\cos\beta_4^{(r)}x+C_4^{(r)}\sinh\beta_4^{(r)}x+D_4^{(r)}\cosh\beta_4^{(r)}x,\ L_3\le x\le L_4\\
W_5^{(r)}(x)&=A_5^{(r)}\sin\beta_5^{(r)}x+B_5^{(r)}\cos\beta_5^{(r)}x+C_5^{(r)}\sinh\beta_5^{(r)}x+D_5^{(r)}\cosh\beta_5^{(r)}x,\ L_4\le x\le L_5\\
W_6^{(r)}(x)&=A_6^{(r)}\sin\beta_6^{(r)}x+B_6^{(r)}\cos\beta_6^{(r)}x+C_6^{(r)}\sinh\beta_6^{(r)}x+D_6^{(r)}\cosh\beta_6^{(r)}x,\ L_5\le x\le L_6
\end{aligned} \quad (14)$$

Mode shapes $W^{(r)}(x)$ and $W^{(s)}(x)$ are orthogonal that is (Sinha 2010)

$$\int_0^L W^{(r)}\left(x\right)W^{(s)}\left(x\right)dx=0,\quad r\neq s \quad (15)$$

where $W^{(s)}\left(x\right)$ is the arbitrary mode shape.

The piezoelectric patch 1, patch 2 cover the beam regions $(L_1\le x\le L_2)$ and $(L_4\le x\le L_5)$ respectively as shown in Fig. 1(a). Hence the second term of Eq. (1.1) is multiplied by $\left[H(x-L_1)-H(x-L_2)\right]$, $\left[H(x-L_4)-H(x-L_5)\right]$ for the region $(L_1\le x\le L_2)$ and $(L_4\le x\le L_5)$ respectively, where $H(x)$ is the heavy side function. The internal bending moment $M_z(x,t)$ for these regions are (Erturk and Inman 2008)

$$M_z(x,t)=E(x)I(x)\frac{\partial^2w^{(r)}(x,t)}{\partial x^2}+\vartheta v_z(t)H_z(x),\ z=1,2 \quad (16.1)$$

The coupling term ϑ and the heavy side function $H_1(x)$ and $H_2(x)$ are given by

$$\vartheta=\frac{E_pd_{31}b}{2t_p}(h_b^2-h_c^2) \quad (16.2)$$

$$\begin{aligned}
H_1(x)&=\left[H(x-L_1)-H(x-L_2)\right],\\
H_2(x)&=\left[H(x-L_4)-H(x-L_5)\right]
\end{aligned} \quad (16.3)$$

where d_{31} is the piezoelectric charge coefficient, b is the

width of the piezoelectric patch, $v_z(t)$ is the voltage across piezoelectric patches. By substituting Eq. (13) in Eq. (1.1) then multiplying both sides by an arbitrary mode shape $W^{(s)}(x)$, integrating it from *0* to *l* and applying the orthogonality conditions given in Eq. (15), the electromechanically coupled ordinary differential equation for the modal response of the harvester is obtained as

$$\Delta\left(\frac{d^2T_z^{(r)}}{dt^2}+2\xi\omega_r\frac{dT_z^{(r)}}{dt}+\omega_r^2T_z^{(r)}(t)\right)+\chi_z v_z(t) = \int_0^L W^{(r)}(x)\,f(x,t)dx \qquad z=1,2 \tag{17.1}$$

where $\Delta = m(x)\int_0^L W^{(r)2}(x)dx = \sum_{n=1}^{6} m_n \int_{L_{n-1}}^{L_n} W_n^{(r)2}(x)dx$ (17.2)

ξ is the damping ratio. χ_1 and χ_2 are the modal coupling term given by

$$\chi_1 = \vartheta\left[\left.\frac{dW_2^{(r)}(x)}{dx}\right|_{x=L_2} - \left.\frac{dW_2^{(r)}(x)}{dx}\right|_{x=L_1}\right],$$
$$\chi_2 = \vartheta\left[\left.\frac{dW_5^{(r)}(x)}{dx}\right|_{x=L_5} - \left.\frac{dW_5^{(r)}(x)}{dx}\right|_{x=L_4}\right] \tag{17.3}$$

A dynamic point force $f(x,t)=F\sin(\omega t)\delta(x-L)$ is applied at the free end of the beam, where ω is the angular frequency of the external dynamic force, *x* is the position on the beam $(0\le x\le L)$, *F* is magnitude of the tip force, $\delta(x-L)$ is the Dirac delta function to model a point force (Wang *et al*. 2012) .

$$\int_0^L W^{(r)}(x)\,f(x,t)dx = \int_0^L W^{(r)}(x)F\sin(\omega t)\delta(x-L)dx = W_6^{(r)}(L)F\sin(\omega t) \tag{17.4}$$

By solving Eq. (17.1), the modal response obtained is

$$T_z^{(r)}(t) = \frac{(W_6^{(r)}(L)F-\chi_z V_z)\sin(\omega t)}{\Delta(\omega_r^2-\omega^2+j2\xi\omega_r\omega)}, \quad z=1,2 \tag{17.5}$$

3.3 Voltage and power analysis

The axial strain is given by (Chen *et al*. 2006)

$$\varepsilon^{(r)}(x,t) = -y_c\frac{\partial^2 w^{(r)}(x,t)}{\partial x^2} \tag{18}$$

Since there is no external electric field applied, the electric field displacement $D^{(r)}(x,t)$ of the piezoelectric patch is expressed as

$$D^{(r)}(x,t) = d_{31}E_p\varepsilon^{(r)}(x,t) \tag{19.1}$$

From Eq. (18) and Eq. (19.1), the electric field displacement of piezoelectric patch is

$$D^{(r)}(x,t) = -d_{31}y_cE_p\frac{\partial^2 w^{(r)}(x,t)}{\partial x^2} \tag{19.2}$$

The electric charge $Q_1^{(r)}(t)$ and $Q_2^{(r)}(t)$ developed from the piezoelectric patch 1 and 2 are obtained by integrating the electric displacement in Eq. (19.2) over the electrode area as

$$Q_1^{(r)}(t) = \int_{L_1}^{L_2} Db\,dx = -\int_{L_1}^{L_2}\left(d_{31}y_cE_pb\frac{\partial^2 W_2^{(r)}(x,t)}{\partial x^2}\right)dx = -d_{31}y_cE_pb\left[\left.\frac{dW_2^{(r)}}{dx}\right|_{x=L_2} - \left.\frac{dW_2^{(r)}}{dx}\right|_{x=L_1}\right]T_1^{(r)}(t) \tag{20.1}$$

$$Q_2^{(r)}(t) = \int_{L_4}^{L_5} Db\,dx = -\int_{L_4}^{L_5}\left(d_{31}y_cE_pb\frac{\partial^2 W_5^{(r)}(x,t)}{\partial x^2}\right)dx = -d_{31}y_cE_pb\left[\left.\frac{dW_5^{(r)}}{dx}\right|_{x=L_5} - \left.\frac{dW_5^{(r)}}{dx}\right|_{x=L_4}\right]T_2^{(r)}(t) \tag{20.2}$$

Let $k_1 = -d_{31}y_cE_pb\left[\left.\frac{dW_2^{(r)}}{dx}\right|_{x=L_2} - \left.\frac{dW_2^{(r)}}{dx}\right|_{x=L_1}\right]$,
$k_2 = -d_{31}y_cE_pb\left[\left.\frac{dW_5^{(r)}}{dx}\right|_{x=L_5} - \left.\frac{dW_5^{(r)}}{dx}\right|_{x=L_4}\right]$ (20.3)

$$Q_z^{(r)}(t) = k_zT_z^{(r)}(t), \quad z=1,2 \tag{20.4}$$

The current $i_z(t)$ and voltage $v_z(t)$ generated from the piezoelectric patches are

$$i_z(t) = \frac{dQ_z^{(r)}(t)}{dt} = \sum_{r=1}^{\infty} k_z\frac{dT_z^{(r)}(t)}{dt}, \quad z=1,2 \tag{21}$$

$$v_z(t) = \sum_{r=1}^{\infty}\frac{Q_z^{(r)}(t)}{C_p}, z=1,2 \tag{22.1}$$

The internal capacitance of the piezoelectric patch is obtained from

$$C_p = \frac{\varepsilon_{33}^s bL_p}{t_p} \tag{22.2}$$

where ε_{33}^s is the permittivity of the piezoelectric patch at constant strain, L_p is the length of the piezoelectric patch. The dimension and properties of piezoelectric patch 1 and 2 are same. The two piezoelectric patches are connected in series and its electrical equivalent circuit is shown in Fig. 2.

The voltage $v_1(t)$ and $v_2(t)$ in Fig. 2 are determined by applying the Kirchhoff current Law, as explained below.

$$\frac{v_1(t)}{R_l}+C_p\frac{dv_1(t)}{dt}+\frac{v_2(t)}{R_l} = i_1(t) \tag{23.1}$$

$$\frac{v_1(t)}{R_l}+\frac{v_2(t)}{R_l}+C_p\frac{dv_2(t)}{dt} = i_2(t) \tag{23.2}$$

Let $T_z^{(r)}(t) = T_z^{(r)}e^{j\omega t}$ and $v_z(t) = V_ze^{j\omega t}$, $z=1,2$

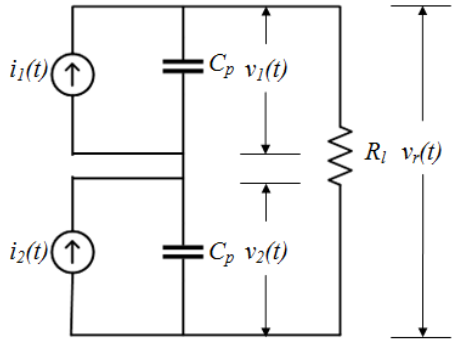

Fig. 2 Electrical equivalent circuit of piezoelectric patches

As the current generated by the piezoelectric patch1 and 2 are different, the output voltage across the load resistor R_l is determined by applying superposition theorem and by substituting $i_1(t)$ and $i_2(t)$ into Eqs. (23.1) and (23.2), the Eq. (23.1) and Eq. (23.2) can be expressed as

$$\left(\frac{1}{R_l}+j\omega C_p\right)V_z - j\omega\sum_{r=1}^{\infty}k_z T_z^{(r)} = 0, \quad z=1,2 \tag{24.1}$$

Substituting the modal response function from Eq. (17.5) in Eq. (24.1), $v_z(t)$ is obtained as below

$$\left(\frac{1}{R_l}+j\omega C_p\right)V_z - j\omega\sum_{r=1}^{\infty}k_z\frac{(W_6^{(r)}(L)F_r-\chi_z V_z)}{\Delta(\omega_r^2-\omega^2+j2\xi\omega_r\omega)} = 0\ , \quad z=1,2 \tag{24.2}$$

$$v_z(t)=\frac{\sum_{r=1}^{\infty}\frac{j\omega k_z F_r W_6^{(r)}(L)}{\Delta(\omega_r^2-\omega^2+j2\xi\omega_r\omega)}}{\frac{1}{R_l}+j\omega C_p+\sum_{r=1}^{\infty}\frac{j\omega k_z\chi_z}{\Delta(\omega_r^2-\omega^2+j2\xi\omega_r\omega)}}\sin\omega t\ , \quad z=1,2 \tag{25.1}$$

where $F_r = F - F_s\frac{L_a}{L}$,

$$F=\frac{N_C I A_C B_p}{2L_{em}}\left(\frac{L_{pm}+d}{\sqrt{R^2+(L_{pm}+d)^2}}-\frac{d}{\sqrt{R^2+d^2}}\right) \tag{25.2}$$

$$F_s=\left(\frac{F}{2L_3^3}\right)\left(3L^2L_a-L_a^3-2L^3\right) \tag{25.3}$$

where L_a is the length of the beam from free end to support position (P), N_c is number of coil turns, I is magnitude of current given to coil, A_c is the cross sectional area of core, B_p is the flux density of the permanent magnet, L_{em} is the length of the electromagnet, L_{pm} is the length of the permanent magnet, R is the radius of the permanent magnet and d is the gap between the magnets as shown in Fig.1 (a). F_s is the magnitude of the reaction force at the support P. There is no external force applied at support (P), the force at this point is the reaction force due to the applied force at the free end. The magnitude (F_s) of reaction force at support (P) is computed by equating the displacement at support P due to the applied force at the free end and the displacement at support (P) due to support reaction. In this work, the voltage generated from the piezoelectric patches due to first mode $(r=1)$ only is considered and from Eq. (25.1) it is derived to be

$$v_z(t)=\frac{j\omega k_z F_r R_l W_6^{(r)}(L)}{\left(1+j\omega R_l C_p\right)\left(\Delta(\omega_r^2-\omega^2+j2\xi\omega_r\omega)\right)+j\omega k_z\chi_z R_l}\sin\omega t\ , \quad z=1,2 \tag{26.1}$$

The magnitude and phase of the output voltage from the piezoelectric patch are

$$V_z=\frac{\omega k_z F_r R_l W_6^{(r)}(L)}{\sqrt{\left(\Delta\left(\omega_r^2-\omega^2-2\xi\omega_r\omega^2C_pR_l\right)\right)^2+\left(\Delta 2\xi\omega_r\omega+\Delta\omega\omega_r^2C_pR_l-\Delta\omega^3C_pR_l+\omega k_z\chi_z R_l\right)^2}}\ , z=1,2 \tag{26.2}$$

$$\phi_z=\frac{\pi}{2}\mathrm{sgn}(k_z)-\tan^{-1}\left(\frac{(2\Delta\xi\omega_r\omega+\Delta\omega\omega_r^2C_pR_l-\Delta\omega^3C_pR_l+\omega k_z\chi_z R_l}{\Delta\left(\omega_r^2-\omega^2-2\xi\omega_r\omega^2C_pR_l\right)}\right),\quad z=1,2 \tag{26.3}$$

The voltage across the resistive load R_l in Fig. (2) is given by

$$v_r(t)=v_1(t)+v_2(t) \tag{26.4}$$

$$\text{Let}\quad v_r(t)=V_R\sin\left(\omega t-\phi\right) \tag{26.5}$$

When no load is connected to the energy harvester i.e. under open circuit condition $(R_l\to\infty)$, the magnitude and phase of the open circuit output voltage from the piezoelectric patch are

$$V_{ocz}=\frac{\omega k_z F_r W_6^{(r)}(L)}{\sqrt{\left(-\Delta 2\xi\omega_r\omega^2C_p\right)^2+\left(\Delta\omega\omega_r^2C_p-\Delta\omega^3C_p+\omega k_z\chi_z\right)^2}}\ , \quad z=1,2 \tag{27.1}$$

$$\phi_{ocz}=\frac{\pi}{2}\mathrm{sgn}(k_z)-\tan^{-1}\left(\frac{(\Delta\omega\omega_r^2C_p-\Delta\omega^3C_p+\omega k_z\chi_z)}{-2\Delta\xi\omega_r\omega^2C_p}\right),\quad z=1,2 \tag{27.2}$$

$$v_{oc}(t)=v_{oc1}(t)+v_{oc2}(t) \tag{27.3}$$

$$v_{oc}(t)=V_{oc}\sin(\omega t-\phi) \tag{27.4}$$

V_{oc} is the maximum value of the open circuit output voltage. The power (P_g) generated from the energy harvester is given by

$$P_g = \frac{V^2}{R_{lopt}} \tag{28}$$

where V is the root mean square(rms) value of $v_r(t)$. The optimum load resistance R_{lopt} of the energy harvester at the open circuit ($R_l \to \infty$) fundamental natural frequency is given by (Erturk 2009)

$$R_{l\,optz} = \frac{2}{\omega C_p}\left[\sqrt{\frac{1-\xi^2+(\gamma_z/2\xi)^2}{\left(1+\gamma_z-\xi^2\right)\left(1+\gamma_z-2\xi^2\right)}}\right], \tag{29}$$

$$z = 1, 2, \quad R_{l\,opt} = \frac{(R_{l\,opt1} + R_{l\,opt2})}{2}$$

The damping coefficient is determined by

$$\xi = \frac{\sqrt{B^2-4AC}-B}{2A}, A = 4\left(1+\upsilon^2\right), B = 4\gamma_1\upsilon, \tag{30.1}$$

$$C = \upsilon^2\gamma^2 - \left(\frac{\gamma_1\upsilon\sigma}{\left|\tilde{\alpha}_1(1)\right|\tilde{\theta}_1}\right)^2$$

$$\upsilon = R_l C_p \omega, \quad \gamma_1 = \frac{\tilde{\theta}_1^2}{C_p\omega^2}, \quad \gamma_2 = \frac{\tilde{\theta}_2^2}{C_p\omega^2}, \tag{30.2}$$

$$\sigma = \frac{\cosh\lambda - \cos\lambda}{\sinh\lambda - \sin\lambda}, \tilde{\theta}_1 = k_1, \tilde{\theta}_2 = k_2$$

where ξ is the damping coefficient, A, B and C are coefficients, $\tilde{\theta}$ is the electromechanical coupling and the values of weighted frequency(λ) changes with the position of the support P. To compute the damping coefficient ξ, for any arbitrary value of load resistance R_l, the output voltage across load $\left|\tilde{\alpha}_1(1)\right|$ at resonance is measured from experimentation. This is carried out for each position of support P and the measured value is used to compute the coefficient C in Eq. (30.1). The damping coefficient ξ is determined from Eq. (30.1) using the values of A, B and C. The damping is assumed to be uniform for all the sections of the harvester, hence the damping coefficient computed for piezoelectric patch 1 is used for piezoelectric patch 2 also. This damping coefficient ξ is used for computing R_{lopt}.

4. Results of theoretical analysis

The performance of the energy harvester shown in Fig. 1(a) is evaluated from the model derived in Section 2. The dimensions and the properties of the beam and the piezoelectric patch are given in Table 1. The piezoelectric patches are bonded at a distance of L_1=0.06L and L_4=0.5L from the fixed end. The variation in the first mode frequency of the energy harvester obtained through simulation when the support position P varied from 0.24L to 0.48L is shown in Fig. 3. The results reveal that the first mode frequency is found to vary linearly with the position of the support P and is found to increase when the support P is moved away from fixed end. The first mode shape of the harvester is found to change with the position of the support P and the results for three different position of support P is shown in Fig. 4. It can be seen from Fig. 4 that the deflection is zero at the support position (P) and the tip deflection gradually decreases when the support (P) is moved away from the fixed end.

For each position of support P, the open circuit output voltage(V_{oc}), voltage across the optimum load resistance (V_R) and the power generated (P_g) from the harvester are computed from Eq. (27.4), Eq. (26.5) and Eq. (28) respectively. The optimum load resistance R_{lopt} is computed using Eq. (29).

Table 1 Dimension and properties of the Aluminum beam and Piezoelectric patch (PZT-5H)

Symbol	Description	Value	Units
L	Length of the beam	500	mm
b	Width of the beam	25	mm
t_b	Thickness of the beam	5.5	mm
E_b	Young's modulus of the beam	71	GP_a
ρ_b	Density of the beam	2700	$Kg\ m^{-3}$
l_p	Length of piezoelectric patch	76.5	mm
b_p	Width of piezoelectric patch	25	mm
t_p	Thickness of piezoelectric patch	0.5	mm
E_p	Young's modulus of piezoelectric patch	47.62	GP_a
ρ_p	Density of piezoelectric patch	7500	$Kg\ m^{-3}$
d_{31}	Piezoelectric charge coefficient	-265	pCN^{-1}

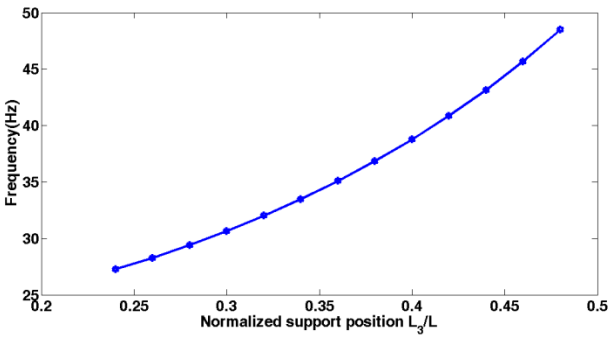

Fig. 3 Variation in first Mode frequency for different position of the support P (Analytical)

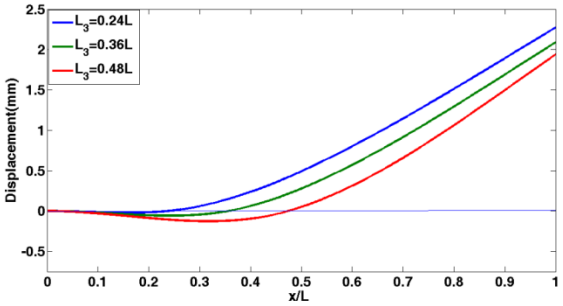

Fig. 4 Results showing change in the first mode shape (Analytical)

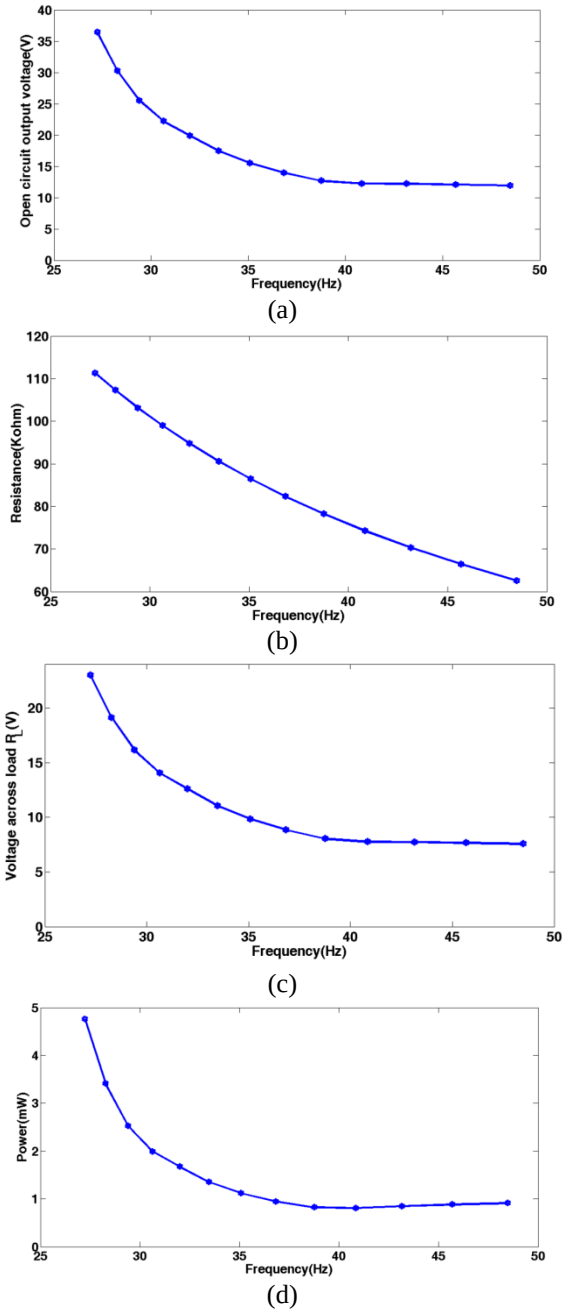

Fig. 5 Results showing performance of the energy harvester with frequency (analytical) (a) Open circuit output voltage (V_{oc}), (b) Load resistance R_l, (c) Voltage across load resistance (V_R) and (d) Power (P_g)

The results in Figs. 5(a)-5(d) shows the variation in V_{oc}, R_{lopt}, V_R and P_g with the frequency, corresponding to the different support position P. The results show that the energy harvester can generate output voltage in wider operating frequency range (broadband). Very fine variation in the support position can produce gradual and continuously varying frequency-voltage characteristics.

5. Experimental results and discussions

The analytical model in section 3 and the results obtained in section 4 are validated experimentally by fabricating the energy harvester. The photograph of the fabricated energy harvester is shown in Fig. 6. The specifications of electromagnetic exciter placed at the tip of the beam are: number of coil turns N_c=2000, length L_{em}=16mm and cross sectional area of the core A_c=78mm^2, flux density of the cylindrical permanent magnet B_p=1.1T, length L_{pm}=10mm, radius R=5mm and the gap between the magnets d=10mm. The harvester is made to vibrate at resonance for each position of the support P by tuning the excitation frequency of the electromagnetic exciter to the first mode frequency corresponds to that position. The amplitude of the excitation signal applied to the exciter is fixed as 10 V peak to peak for all position of support P. The first mode frequency of the energy harvester for different position of support P measured experimentally is compared with the frequency obtained from the analytical model and is shown in Fig. 7. It is observed that the first mode frequency is found to vary from 27.24 Hz to 48.47 Hz in simulation and 26.63 Hz to 48.71 Hz in experimentation when the position of the support P is varied from 0.24 L to 0.48L from the fixed end. The input to the electromagnetic exciter is applied from the arbitrary waveform generator (Agilent 33500B) and the output from the piezoelectric patches is measured using digital storage oscilloscope (Agilent DSO1002A). During experimentation, the overhang length is varied by moving the support position P. For each support position P, the optimum value of load resistance R_{lopt} is calculated from Eq. (29) and connected across the output of the piezoelectric patches. In experimentation, for each support position P the resonance frequency, the corresponding open circuit voltage (V_{oc}) and the voltage (V_R) across the load resistance R_{lopt} are measured. The measured voltage V_R is used to compute the harvested power using Eq. (28). The results in Figs. 8(a)-8(c) show the comparison of experimental and analytical results of V_{oc}, V_R and P_g with the frequency corresponding to each support position P. From the above results, it is concluded that the experimental results are in close agreement with the results obtained from analytical model. The relative error between the analytical and experimental results in resonant frequency, V_{oc} and V_R for different position of the support P for the harvester is found to be less than -2.23% , -6.19% and -8.6% respectively. Moreover, the variation in generated voltage and harvested power is continuous with gradual variation in magnitude over the operating frequency range.

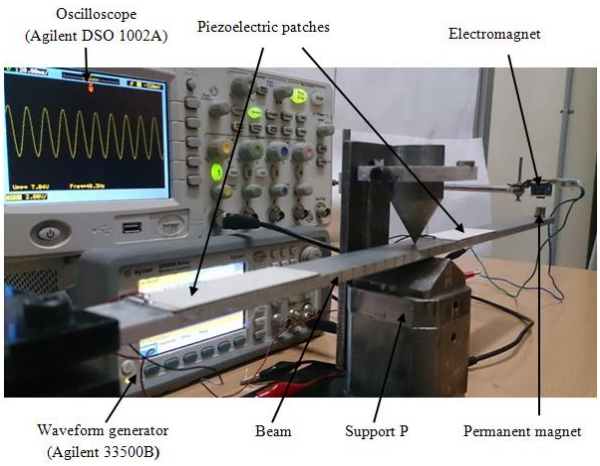

Fig. 6 Photograph of the fabricated broadband energy harvester

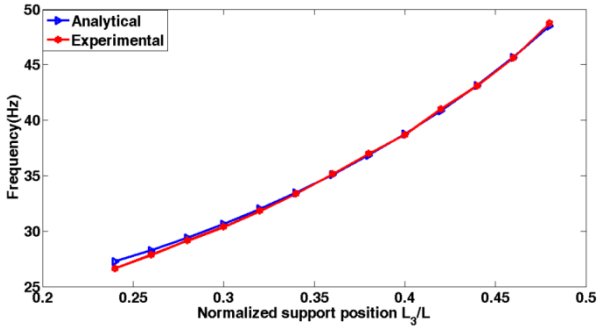

Fig. 7 Comparison of first mode frequency of the energy harvester

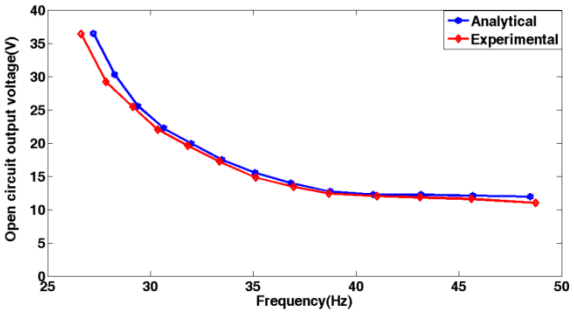

(a)

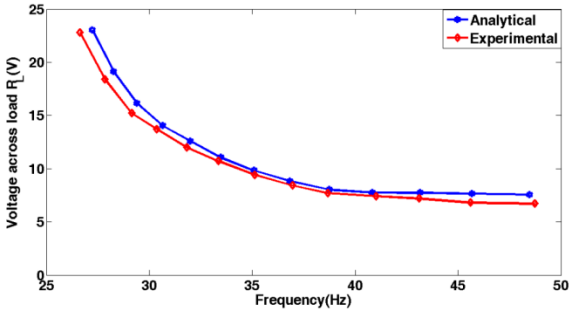

(b)

Continnued-

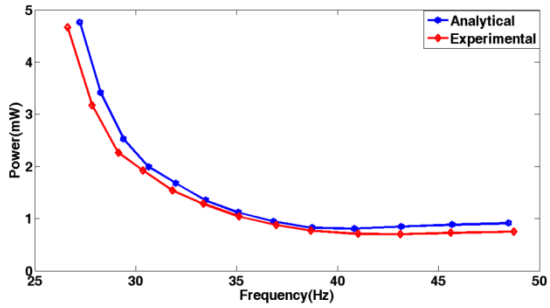

(c)

Fig. 8. Comparison of the performance of the energy harvester with frequency (a) Open circuit output voltage (V_{oc}), (b) Voltage across load resistance (V_R) and (c) Power (P_g)

6. Conclusions

A piezoelectric broadband energy harvester using propped cantilever beam with variable overhang length is designed, analytically modeled using Euler Bernoulli beam theory and experimentally investigated. Results from the analytical model reveal that the mode frequency is a function of the position of the support and the change in the first mode frequency is found to be linear. The proposed broadband energy harvester is relatively simple in design for increasing the operating frequency range. The proposed design does not involve any structural modifications or tailoring, additional structural elements like tip mass or slider mass etc., for altering the resonance frequency for obtaining the broadband. The modeling of the proposed harvester is simple as it requires only few modifications in the boundary and continuity conditions of the regular cantilever piezoelectric energy harvester. The harvester generates the open circuit output voltage ranging from 36.44 V to 11.94 V (from analytical) and 36.4 V to 11.01 V (from experimentation) in the frequency range of 27.2Hz to 48.47 Hz (from analytical) and 26.63 Hz to 48.7 Hz (from experimentation) for the variation in the support position from 0.24 L to 0.48 L. The results from the analytical model and experimentation demonstrate that the energy harvester can be used in wider operating frequency range. The output voltage generated and the power harvested by the energy harvester in the operating frequency range is considerable in magnitude and hence can be used to source electronic circuits and wireless sensor nodes. The proposed harvester produces continually and gradually varying output voltage and power in the operating frequency range. It is finally remarked that as the results obtained are promising, the next step is to work on the design and fabrication of active and passive tuning device which will move the support P in accordance with the variance in the ambient vibration frequency.

References

Anton, S.R. and Sodano, H.A. (2007), "A review of power harvesting using piezoelectric materials (2003–2006)", *Smart Mater. Struct.*, **16**(3), 1-21.

Beeby, S.P., Tudor, M.J. and White, N.M. (2006), "Energy harvesting vibration sources for microsystems applications", *Meas. Sci. Technol.*, **17**(12), 175-195.

Chen, SN., Wang, GJ., Chien, MC. (2006), "Analytical modeling of piezoelectric vibration-induced micro power generator, *Mechatronics*, **16**(7), 379–387

Dong, L., Prasad, M.G. and Fisher, F.T. (2016), "Two-dimensional resonance frequency tuning approach for vibration-based energy harvesting", *Smart Mater. Struct*., **25**(6), 065019 (14pp).

Erturk, A. (2009), "Electromechanical modelling of piezoelectric energy harvesters", Ph.D thesis, Virginia Tech, Blacksburg.

Erturk, A. and Inman, D.J. (2008), "A distributed parameter electromechanical model for cantilevered piezoelectric energy harvesters", *J Vib Acoust*, **130**(4), 041002(15pp).

Erturk, A., Renno, J.M. and Inman, D.J. (2009), "Modeling of Piezoelectric Energy harvesting from an L shaped beam mass structure with an application to UAVs", *J. Intel. Mat. Syst. Str.*, **20**(5), 529-544

Hoffmann, D., Willmann, A., Hehn, T., Folkmer, B. and Manoli, Y. (2016), "A self-adaptive energy harvesting system", *Smart Mater. Struct*., **25**(3), 035013 (10pp).

Kim, H.S., Kim, J.H. and Kim, J. (2011), "A review of piezoelectric energy harvesting based on vibration", *Int. J. Precis. Eng. Manuf.*, **12**(6), 1129-1141.

Kim, IH., Jung, HJ., Lee, B.M. and Jang, S.J. (2011), "Broadband energy harvesting using two degree of -freedom vibrating body", *Appl. Phys. Lett*., **98**(21), 214102(3pp).

Li, P., Liu, Y., Wang, Y., Luo, C., Li, G., Hu, J., Liu, W. and Zhang, W. (2015), "Low-frequency and wideband vibration energy harvester with flexible frame and interdigital structure", *AIP Advances*, **5**(4), 047151(8pp).

Murphy, J.F. (1997), "Transverse vibration of a simply supported beam with symmetric overhang of arbitrary length", *J. Test Eval*., **25**(5), 522-524.

Niri, E.D. and Salamone, S. (2012), "A passively tunable mechanism for a dual bimorph energy harvester with variable tip stiffness and axial load", *Smart Mater. Struct.*, **21**(12), 125025(15pp).

Ou, Q., Chen, X.Q., Gutschmidt, S., Wood, A., Leigh, N. and Arrieta, A.F. (2012), "An experimentally validated double-mass piezoelectric cantilever model for broadband vibration-based energy harvesting", *J. Intel. Mat. Syst. Str.*, **23**(2), 117-126.

Peters, C., Maurath, D., Schock, W., Mezger, F. and Manoli, Y. (2009), "A closed-loop wide-range tunable mechanical resonator for energy harvesting systems", *J. Micromech. Microeng*., **19**(9), 094004(9pp).

Qi, S., Shuttleworth, R., Oyadiji, S.O. and Wright, J. (2010), "Design of multiresonant beam for broadband piezoelectric energy harvesting", *Smart Mater. Struct*., **19**(9), 094009 (10pp)

Salehi-Khojin, A., Bashash, S. and Jalili, N. (2008), "Modeling and experimental vibration analysis of nanomechanical cantilever active probes", *J. Micromech. Microeng*., **18**(8), 085008 (11pp).

Santhosh kumar, B.V.M.P., Suresh, K., Varun Kumar, U., Uma, G. and Umapathy, M. (2012), "Resonance based DC current sensor", *Measurement*, **45**(3), 369-374.

Shahruz, S.M. (2008), "Design of mechanical band-pass filters for energy scavenging: multi-degree-of freedom models", *J. Vib. Control*, **14**(5), 753-768.

Sinha, A. (2010), "Vibration of Mechanical Systems" Cambridge University press, Cambridge, New York,

Su, W.J., Zu, J. and Zhu, Y. (2014), "Design and development of a broadband magnet-induced dual-cantilever piezoelectric energy harvester", *J. Intel. Mat. Syst. Str*., **25**(4) 430-442.

Tang, L., Yang, Y. and Soh, C.K. (2010), "Toward broadband vibration-based energy harvesting", *J. Intel. Mat. Syst. Str*., **21**(18), 1867-1897.

Wang, Q. and Wu, N. (2012), "Optimal design of a piezoelectric coupled beam for power harvesting", *Smart Mater. Struct*., **21**(8), 085013 (9pp).

Wu, H., Tang, L., Yang, Y. and Soh, C.K. (2013), "A novel two degrees of freedom piezoelectric energy harvester", *J. Intel. Mat. Syst. Str.*, **24**(3), 357-368.

Xue, H., Hu, Y. and Wang, Q.M. (2008), "Broadband piezoelectric energy harvesting devices using multiple bimorphs with different operating frequencies", *IEEE T. Ultrason. Ferr*., **55**(9), 2104-2108.

Yang, Z. and Yang, J. (2009), "Connected vibrating Piezoelectric Bimorph beams as a wide-band piezoelectric power harvester ", *J. Intel. Mat. Syst. Str.*, **20**(5), 569-574.

Zhou, W., Penamalli, G.R. and Zuo, L. (2012), "An efficient vibration energy harvester with a multi-mode dynamic magnifier", *Smart Mater. Struct*., **21**(1)**,** 015014 (9pp)

Zhu, D., Tudor, M.J. and Beeby, S.P. (2010), "Strategies for increasing the operating frequency range of vibration energy harvesters: a review", *Meas. Sci. Technol*., **21**(2), 022001 (29pp).

Zhu, Y., Zu, J. and Su, W. (2013), "Broadband energy harvesting through a piezoelectric beam subjected to dynamic compressive loading", *Smart Mater. Struct*., **22**(4), 045007 (13pp).

HJ